Title

Peptidoglycan Synthesis Machinery in Agrobacterium tumefaciens During Unipolar Growth and Cell Division

Journal

mBio, 5(3)

ISSN

2161-2129

Authors

Cameron, Todd A
Anderson-Furgeson, James
Zupan, John R
et al.

Publication Date

2014-07-01

DOI

10.1128/mbio.01219-14

Peer reviewed

Peptidoglycan Synthesis Machinery in *Agrobacterium tumefaciens* During Unipolar Growth and Cell Division

Todd A. Cameron, James Anderson-Furgeson, John R. Zupan, Justin J. Zik, Patricia C. Zambryski

Department of Plant and Microbial Biology, University of California, Berkeley, California, USA

ABSTRACT **The synthesis of peptidoglycan (PG) in bacteria is a crucial process controlling cell shape and vitality. In contrast to bacteria such as *Escherichia coli* that grow by dispersed lateral insertion of PG, little is known of the processes that direct polar PG synthesis in other bacteria such as the *Rhizobiales*. To better understand polar growth in the *Rhizobiales Agrobacterium tumefaciens*, we first surveyed its genome to identify homologs of (~70) well-known PG synthesis components. Since most of the canonical cell elongation components are absent from *A. tumefaciens*, we made fluorescent protein fusions to other putative PG synthesis components to assay their subcellular localization patterns. The cell division scaffolds FtsZ and FtsA, PBP1a, and a *Rhizobiales*- and *Rhodobacterales*-specific L,D-transpeptidase (LDT) all associate with the elongating cell pole. All four proteins also localize to the septum during cell division. Examination of the dimensions of growing cells revealed that new cell compartments gradually increase in width as they grow in length. This increase in cell width is coincident with an expanded region of LDT-mediated PG synthesis activity, as measured directly through incorporation of exogenous D-amino acids. Thus, unipolar growth in the *Rhizobiales* is surprisingly dynamic and represents a significant departure from the canonical growth mechanism of *E. coli* and other well-studied bacilli.**

IMPORTANCE **Many rod-shaped bacteria, including pathogens such as *Brucella* and *Mycobacterium*, grow by adding new material to their cell poles, and yet the proteins and mechanisms contributing to this process are not yet well defined. The polarly growing plant pathogen *Agrobacterium tumefaciens* was used as a model bacterium to explore these polar growth mechanisms. The results obtained indicate that polar growth in this organism is facilitated by repurposed cell division components and an otherwise obscure class of alternative peptidoglycan transpeptidases (L,D-transpeptidases). This growth results in dynamically changing cell widths as the poles expand to maturity and contrasts with the tightly regulated cell widths characteristic of canonical rod-shaped growth. Furthermore, the abundance and/or activity of L,D-transpeptidases appears to associate with polar growth strategies, suggesting that these enzymes may serve as attractive targets for specifically inhibiting growth of *Rhizobiales*, *Actinomycetales*, and other polarly growing bacterial pathogens.**

Received 18 April 2014 **Accepted** 24 April 2014 **Published** 27 May 2014

Citation Cameron TA, Anderson-Furgeson J, Zupan JR, Zik JJ, Zambryski PC. 2014. Peptidoglycan synthesis machinery in *Agrobacterium tumefaciens* during unipolar growth and cell division. mBio 5(3):e01219-14. doi:10.1128/mBio.01219-14.

Editor Caroline Harwood, University of Washington

Address correspondence to Patricia C. Zambryski, zambrysk@berkeley.edu.

This article is a direct contribution from a member of the American Academy of Microbiology.

Peptidoglycan (PG) is a fundamental feature of nearly all bacteria and plays a primary role in maintaining cell integrity and cell shape. The PG layer is an interconnected mesh in the bacterial cell envelope, and, when isolated intact from a cell, the sacculus it forms retains the overall, albeit deflated, shape of the original cell. PG is composed of glycan strands covalently bonded by short, periodic peptide cross-links. In bacilli, the glycan strands run roughly perpendicularly to the long axis of the cell, with peptide cross-links arranged in parallel to the cell axis (1–4). This architecture allows bacteria to withstand significant osmotic pressure, and thicker cell walls confer greater resistance: typical Gram-negative strains can withstand ~2 to ~5 atm, whereas Gram-positive strains with thicker cell walls can withstand upward of 20 atm (5, 6).

To grow and divide, bacteria must enlarge and remodel this PG mesh. For cell division, most bacteria in which this has been studied share the same strategy: PG is synthesized at the midcell in a decreasing diameter until the cell is completely bisected and two separate cells are formed (7). In *Escherichia coli*, septal PG synthesis is conducted by a divisome consisting of the transpeptidase PBP3, the transglycosylase/transpeptidase PBP1b, various PG-remodeling enzymes, and an assortment of regulatory and structural proteins (8). These components are all organized along a large scaffolding ring formed by the tubulin homolog FtsZ, and contraction of this ring provides the force that propels the division process (9–11). In most bacteria, FtsZ is thought to be anchored to the cytoplasmic membrane by FtsA.

While bacteria employ a variety of strategies to expand their cell wall prior to division, in general, new PG is inserted either in a laterally dispersed fashion along the cell length or at specific landmarks such as the cell pole(s) (12). The most popular bacterial model systems, including *E. coli*, *Bacillus subtilis*, and *Caulobacter*

crescentus, utilize the laterally dispersed mode of PG insertion, leading to a substantial body of research and understanding of this type of cell elongation. In *E. coli*, lateral PG synthesis is conducted by an elongasome consisting primarily of the transpeptidase PBP2 and the transglycosylase/transpeptidase PBP1a plus several accessory proteins. These are likely organized by short filaments of the actin homolog MreB and associated structural proteins (13, 14).

In contrast, relatively little is known about the components and processes that facilitate polar growth even though this growth strategy is utilized by several orders of bacteria, notably, the *Actinomycetales* and the *Rhizobiales*, and sporadically among other bacterial species (12, 15–17). Polar growth in the Gram-negative *Rhizobiales* has only recently been explored, and unlike the *Actinomycetales*, the *Rhizobiales* grow only from one pole. Although unipolar growth produces new and old cells that are roughly equivalent in size after division, some asymmetries are present; for example, the old poles of *Agrobacterium tumefaciens* can produce a holdfast (16). Members of the *Rhizobiales* also lack the lateral PG synthesis scaffold MreB and other related proteins such as MreC, MreD, RodA, and RodZ that are essential in the well-studied model systems mentioned above (12, 18, 19). However, the cell division proteins FtsA and FtsZ both localize to the growth pole and the septum in *A. tumefaciens*, suggesting that these well-known cell division components may also participate in polar growth (20).

Here we investigated whether other classical divisome-specific PG synthesis components might also localize to the growth pole in *A. tumefaciens*. Surprisingly, FtsZ and FtsA were the only cell division components to exhibit robust localization to the growth pole. Several penicillin binding proteins (PBPs) with D,D-transpeptidase (DDT) activity exhibited only transient polar localization. However, *A. tumefaciens* and other *Rhizobiales* are enriched in genes encoding L,D-transpeptidases (LDTs), one of which showed strong localization to the growing pole. Finally, the area of PG synthesis activity at the polar tip gradually expanded distally as cells elongated such that most of the new cell compartment was engaged in PG synthesis. This expanded activity appeared concomitantly with an increase in the width of the entire new cell compartment and resulted in old and new cell compartments with approximately equivalent lengths and widths just prior to cell division.

RESULTS

***Agrobacterium* lacks the rod-shaped cell elongation machinery.** To understand the molecular components responsible for polar growth in *A. tumefaciens*, the genome of the wild-type strain C58 was first examined for homologs of the well-studied cell elongation machinery of *C. crescentus* and *E. coli*. Although an earlier search in *A. tumefaciens* failed to find homologs to the canonical cell elongation scaffold proteins MreB, MreC, MreD, RodA, and RodZ (19), we took advantage of updated sequence databases and improved tools to reexamine the genome; no additional homologs of these proteins were identified in our search. However, this result prompted us to perform an exhaustive bioinformatics search through the *A. tumefaciens* genome for all types of proteins reportedly involved in bacterial cell growth; a survey of over 70 of these proteins is presented in Table S1 in the supplemental material.

Our bioinformatics analyses revealed clear or likely homologs of the highly conserved cytoplasmic PG precursor synthesis machinery, most cell division components, and a suite of carboxy- and endopeptidases, lytic transglycosylases, and amidases. Most notably, an unusual enrichment in putative L,D-transpeptidase enzymes, three copies of FtsZ (20), and two copies each of PBP3, PBP1b, and FtsK were found. In further support of the interpretation that polar elongation utilizes a novel pathway, we found no homologs of the cell elongation-specific transpeptidase PBP2. Of all the canonical cell elongation components, only the transglycosylase/transpeptidase PBP1a remained present in *A. tumefaciens.*

Further phylogenetic analyses of the homologs of PBP1, PBP2, and PBP3 (PBP1/2/3) of *A. tumefaciens* compared to homologs in related *Proteobacteria* supported our interpretation of a duplication of PBP3 and PBP1b, the presence of PBP1a and PBP1c, and the absence of PBP2 (see Fig. S1 and S2 in the supplemental material). Surprisingly, the presumed PBP1b of *A. tumefaciens* and other *Alphaproteobacteria* formed a distinct clade that was paraphyletic with PBP1b of *E. coli*. Within the *Alphaproteobacteria*, these proteins form a third major clade beside PBP1a and PBP1c and are therefore referred to here as PBP1b.

FtsZ and FtsA likely contribute to polar growth. Since *A. tumefaciens* lacks the expected cell elongation machinery, the polar growth process is likely mediated by some combination of cell division components and novel proteins. To investigate this hypothesis, we first focused on localizing two important cell division scaffolding proteins: the actin homolog FtsA and the tubulin homolog FtsZ. Our previous studies monitored snapshots of cells at different stages of the cell cycle and revealed that FtsA-green fluorescent protein (FtsA-GFP) and FtsZ-GFP localize both to the cell pole during polar growth and to the midcell during cell division. Since FtsZ localization appeared more variable than FtsA localization, here we asked to what degree their localization is coordinated over the cell cycle and whether they sometimes have distinct localization patterns or potentially independent roles.

To this end, we performed a quantitative study of FtsA-GFP and FtsZ-GFP localization over the cell cycle. Whole-cell fluorescence profiles of unsynchronized cells were represented as demographs to reveal population-level trends in protein localization at various cell lengths (21, 22). Demographs are an ideal approach for examining the localization of cell division proteins such as FtsZ, since their behavior is closely tied to cell geometry rather than cell age (23–25). To construct demographs, fluorescent profiles of several hundred cells were collected and graphed as single lines stacked according to cell length, using a custom R script (see Materials and Methods). Given sufficient sampling, such a graph will roughly represent progression through the cell cycle, using cell length as a proxy for elapsed time. Since the shortest (new) cells are at the top and the longest (dividing) cells are at the bottom, the relative timings of cell cycle-dependent localization can be inferred from this ordered distribution of cell lengths. To orient old versus new poles for the demographs presented here, we used FM4-64, a lipophilic dye that preferentially labels old poles in *A. tumefaciens* (20). As shown in Fig. 1A, FtsZ-GFP progressed through three overall localization patterns: an initial polar localization, a mix of lateral and diminishing polar foci, and, finally, intense midcell localization.

In contrast, the FtsA-GFP demograph (Fig. 1B) shows that FtsA-GFP remained exclusively at the growth pole until just prior to cell division. Comparison of the FtsA-GFP and FtsZ-GFP demographs revealed that FtsA-GFP consistently remained at the growth pole during the times when FtsZ-GFP localized to numerous sites throughout the cell and at cell poles. Once FtsZ-GFP

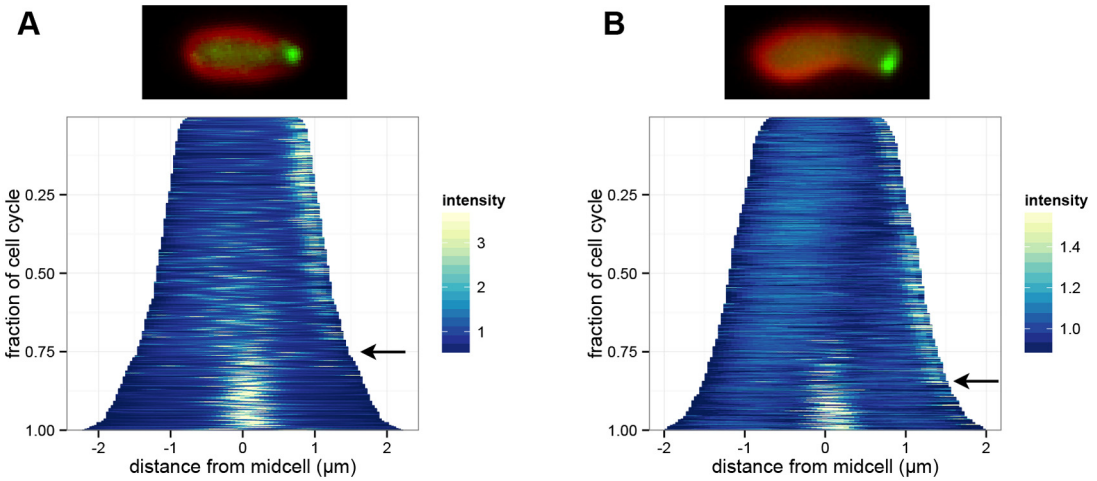

FIG 1 FtsZ and FtsA colocalize to the growth pole over most of the cell cycle but exhibit different timings in the transition to midcell localization. (A and B) (Upper panels) Examples of cells labeled with FM4-64 expressing either FtsZ-GFP (A) or FtsA-GFP (B). FM4-64 most intensely labeled the old pole opposite the FtsZ and FtsA fluorescent foci. (Lower panels) Demographs of cells expressing either FtsZ-GFP or FtsA-GFP. Arrows indicate a transition to consistent midcell localization. Demographs are oriented with the growing pole on the right, using FM4-64 old pole labeling as a reference.

localized to the midcell in longer cells (representing the latter stages of the cell cycle), it no longer localized to the poles or other locations in the cell. In contrast, FtsA-GFP localized briefly to both the pole and the midcell as cells transitioned to septal growth. Furthermore, FtsZ-GFP appeared at the midcell before FtsA-GFP (black arrows, Fig. 1). Given an ~95-min doubling time for *A. tumefaciens*, FtsZ-GFP localized to the midcell 9 to 10 min before FtsA-GFP. The longest 15% of cells showed similar midcell localizations of both FtsA-GFP and FtsZ-GFP just prior to cell division. Finally, these results are consistent with our previous time-lapse data for FtsA-GFP (20) and demonstrate the validity of using demographs to examine the localization of as-yet-untested proteins through the cell cycle.

Contributions of PBPs to polar growth. Given that the cell division scaffolding proteins FtsA and FtsZ both localize to the growth pole, we next investigated whether cell division PG synthesis proteins might also localize to the growth pole. To gain a global perspective of the localization of all *A. tumefaciens* PBPs, cells were treated briefly with BocillinFL, a fluorescent penicillin derivative commonly used for *in vitro* detection of PBPs. BocillinFL treatment revealed weak but consistent polar labeling and stronger midcell labeling (Fig. 2A and B). Midcell BocillinFL labeling occurred in the longest ~25% of cells in a manner coincident with the frequency and distribution of midcell localization of FtsZ-GFP (see Fig. 1A). The strong midcell labeling of BocillinFL provides support for our previous observation that treatment with carbenicillin, a penicillin derivative that targets DDTs, results in morphology defects at the midcell but does not affect the cell poles (20). These data together suggest that PBPs predominantly act at the midcell. To further test the role of PBPs in polar growth, we made fluorescent fusions to several of the *A. tumefaciens* PBPs.

We hypothesized that *A. tumefaciens* may still utilize PBP1a as a transglycosylase for polar elongation despite its lacking the cell elongation transpeptidase PBP2. Indeed, a citrine-PBP1a fusion demonstrated a distinct preference for the growth pole over most of the cell cycle (see Fig. S3A and B in the supplemental material), and PBP1a likely accounts for some of the polar BocillinFL labeling observed. Unlike FtsA-GFP or FtsZ-GFP, citrine-PBP1a did not relocalize to the midcell until the final 5% to 10% of the cell cycle, suggesting that it is not needed to initiate cell division.

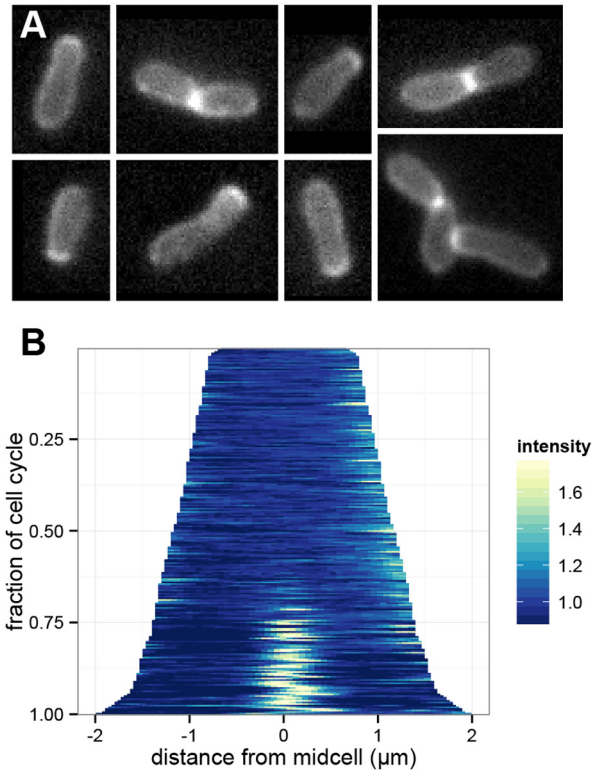

FIG 2 BocillinFL exhibits growth pole and midcell fluorescence. (A and B) Single cells (A) and demograph of cells labeled with BocillinFL (B). Midcell fluorescence is much more intense than growth pole fluorescence, suggesting that a minority of PBPs are involved in polar growth. The demograph is oriented with the growing pole on the right, using FM4-64 labeling of the old pole as a reference.

As noted above, *A. tumefaciens* has two PBP3 transpeptidases, referred to here as PBP3a (Atu2100) and PBP3b (Atu1067). The gene encoding PBP3a is located adjacent to *murE*, *ftsZ*, and *ftsA*, in the same position as *ftsI* (PBP3) in *E. coli*, while the gene for PBP3b is located elsewhere in the genome. To test if either copy of PBP3 might serve as a transpeptidase for polar cell growth, citrine fusions for each protein were examined. Both proteins primarily localized at the septum in long cells, with occasional weak localization to the growth pole in shorter cells (see Fig. S3C and E in the supplemental material). Demographs revealed that citrine-PBP3a very rarely localized to the pole, whereas citrine-PBP3b exhibited polar localization through the first third of the cell cycle (Fig. S3D and F). However, a deletion of PBP3b had no apparent effect on the growth rate (Fig. S3G), suggesting that neither PBP3b nor its localization to the pole is an essential feature of polar growth.

In summary, the weak polar labeling with BocillinFL, PBP1a, and PBP3a/b suggests that PBP-type enzymes are not the major factors responsible for polar PG synthesis. Furthermore, neither PBP3a nor PBP3b remained at the cell poles for the majority of the cell cycle. Thus, we next searched for additional types of transpeptidases that might be required for polar growth.

L,D-Transpeptidases have a major role in polar growth. As noted above, *A. tumefaciens* and other members of the polarly growing *Rhizobiales* contain an unusual abundance of putative L,D-transpeptidase (LDT) proteins (see Table S2 in the supplemental material), suggesting a possible link between LDTs and polar growth. Unlike the PBP2 and PBP3 D,D-transpeptidases (DDTs) that form 4,3-cross-links between D-alanine and m-Dap in two PG stem peptides, LDTs catalyze 3,3-cross-links directly between two m-Dap residues and are insensitive to most penicillins (see reference 26 for a review). More than 50% of the peptide cross-links in *A. tumefaciens* and the related *Rhizobiales Sinorhizobium meliloti* are 3,3-cross-links (16) compared to only 10% in *E. coli* (27). Given our DDT results discussed above, we asked instead if LDTs play a role in polar growth in *A. tumefaciens*.

To understand how the LDTs of the *Rhizobiales* are related to those found in other bacteria, we constructed a phylogenetic tree of the LDTs from over forty bacterial species (see Fig. S4 in the supplemental material) primarily representing alphaproteobacterial strains and select representatives from other *Proteobacteria* and more-divergent species. Table S2 in the supplemental material lists the strains used to construct this tree. For clarity, a smaller tree of the LDTs from twelve *Proteobacteria* is presented in Fig. 3. In contrast with most of the bacteria examined, the LDTs of *A. tumefaciens* (Fig. 3, blue boxes) and other *Rhizobiales* are distributed throughout the tree and are particularly abundant within a few adjacent branches. Closer inspection revealed that these branches (Fig. 3, within green oval) are specifically composed of LDTs found in the two closely related orders of *Rhizobiales* and *Rhodobacterales*. The *Rhizobiales* strains examined typically include about five to eight LDTs in this group, or roughly half the total number of LDTs in each strain.

A subset of the *A. tumefaciens* LDTs were selected for localization studies to sample the various phylogenetic branches and to test the LDTs that were most highly expressed in transcriptome studies (28). A C-terminal superfolding GFP (sfGFP) (29, 30) fusion to Atu0845, one of the *Rhizobiales*/*Rhodobacterales*-specific LDTs, exhibited a striking localization to the growth pole (Fig. 4). Furthermore, the intensity of the growth-pole-localized Atu0845-sfGFP appeared to increase gradually over the cell cycle (Fig. 4B; compare the poles of long cells to those of short cells) and remained at the growth pole despite the appearance of additional septal labeling just prior to cell division. This polar retention may explain the presence of the less intense fluorescence also visible at the old poles in many cells. Figure S5 in the supplemental material diagrams how such bipolar fluorescence could arise as cells divide.

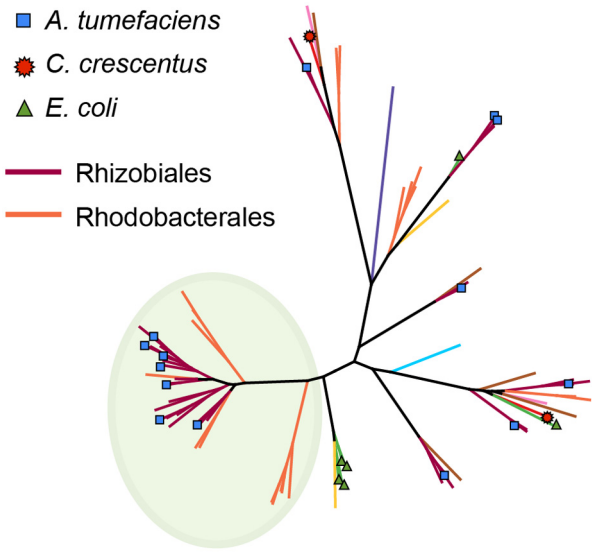

FIG 3 Unrooted phylogenetic tree of LDTs from representative *Proteobacteria* species. The green-shaded area highlights a clade composed only of members of the *Rhizobiales* and *Rhodobacterales* orders. The LDTs from *A. tumefaciens* (blue squares), *C. crescentus* (red stars), and *E. coli* (green triangles) are indicated on the tree. Branches are colored according to the taxonomic order of the strains: multiple orders (black), *Rhizobiales* (burgundy), *Rhodobacterales* (orange), *Sphingomonadales* (brown), *Caulobacterales* (red), *Rhodospirillales* (pink), *Neisseriales* (turquoise), *Pseudomonadales* (yellow), *Enterobacteriales* (green), and *Campylobacterales* (purple). The results of a more extensive analysis are presented in Fig. S4 in the supplemental material.

The other LDTs tested did not exhibit strong polar localization when fused to sfGFP. Instead, these LDTs tended to predominantly localize to the midcell at cell division and then localize temporarily at the new pole in newly divided cells (see Fig. S6A to D in the supplemental material), as seen with the citrine-PBP3b fusion. One fusion, Atu1164-sfGFP, localized heterogeneously along the membrane irrespective of the cell cycle or growth pole (see Fig. S6E). Atu0669-sfGFP, the other *Rhizobiales*/*Rhodobacterales* clade representative, gained localization to the growth pole immediately prior to cell division (see red circle in Fig. S6B). The weaker and more diffuse localization of these four LDTs contrasts with the strong polar localization of Atu0845-sfGFP.

Localization of PG synthesis activity. The above results indicate that PG synthesis enzymes and scaffolding proteins localize to the growth pole or midcell and, in the case of FtsZ, to multiple sites throughout *A. tumefaciens*, and yet it is not clear at which location(s) PG synthesis is most active. To address this issue, we took advantage of the fact that many bacteria readily incorporate exogenous D-amino acids into their PG (31, 32). Incorporation into existing PG is mediated either by DDTs, which exchange the exogenous amino acid with the fifth D-alanine in the stem peptide, or by LDTs, which act on the fourth position D-alanine (32). In *A. tumefaciens*, mass spectrometry studies indicate that exogenous D-amino acid analogs are specifically incorporated into the fourth stem peptide position (33), suggesting the involvement of LDTs.

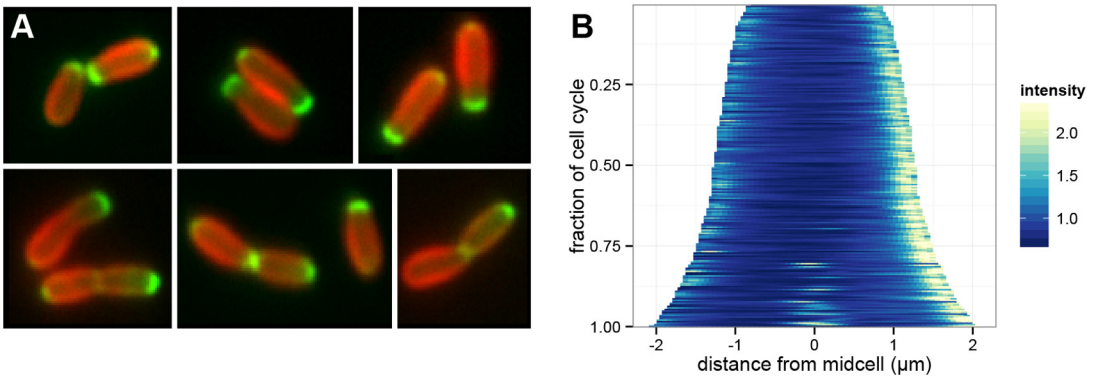

FIG 4 LDT Atu0845 localizes intensely to the growth pole. (A) Single cells expressing Atu0845-sfGFP and labeled with FM4-64. (B) Demograph of cells expressing Atu0845-sfGFP. Growth poles are oriented to the right, using FM4-64 old pole labeling as a reference. A model for the generation of Atu0845-sfGFP fluorescence at the old pole is presented in Fig. S5A in the supplemental material.

To directly visualize where LDTs are most active, we grew cells with exogenously added alkyne-D-alanine (alkDala), a D-alanine analog that can readily be covalently linked *in situ* to an azido-fluorophore using a simple copper-catalyzed click chemistry protocol (34). Fluorescence microscopy revealed that cells were labeled at one pole or were labeled at the midcell in obviously constricting cells (Fig. 5A). Similar results were reported using azido-D-alanine and prelabeled fluorescent D-alanine probes in *A. tumefaciens* (33).

Growth pole labeling of alkDala was confirmed using a pulse-chase with Texas red succinimidyl ester (TRSE). TRSE nonspecifically labels surface proteins and is retained specifically with previously synthesized cell material in *A. tumefaciens* (16). After incubation with TRSE, AlkDala labeling specifically targeted the regions of new growth that were unlabeled by TRSE (see Fig. S7A in the supplemental material). Additionally, fluorescent vancomycin, a commonly used probe for nascent PG, demonstrated the same labeling patterns (polar and midcell) as alkDala when combined with a TRSE chase (see Fig. S7B). Thus, alkDala exchange occurs in proximity to nascent PG synthesis.

Unexpectedly, despite the fact that all of the cells were incubated with alkDala for the same length of time, the labeled region was noticeably larger in longer cells than in shorter cells (Fig. 5A). This change was quantified by measuring the length of the region of alkDala labeling from the growth pole to the point where the fluorescence labeling plateaued to cellular background intensities. In cells without midcell alkDala labeling (cells less than ~3.0 μm in length), the size of the labeling region increased linearly in relation to cell length and roughly doubled in length as cells grew (red line, Fig. 5B). After the appearance of midcell labeling (cells greater than ~3.0 μm in length), the ratio of labeling area to cell length appeared to increase at a slightly higher rate than before, perhaps reflecting additional septal PG synthesis activity (blue line, Fig. 5B). A demograph of these cells displays dramatically increased alkDala labeling along the length of the new cell compartments prior to cell division (see Fig. S7C in the supplemental material). Thus, while the growth of the new pole appears to initially concentrate at the polar tip, it expands to include participation from most of the new cell compartment by the time of cell division.

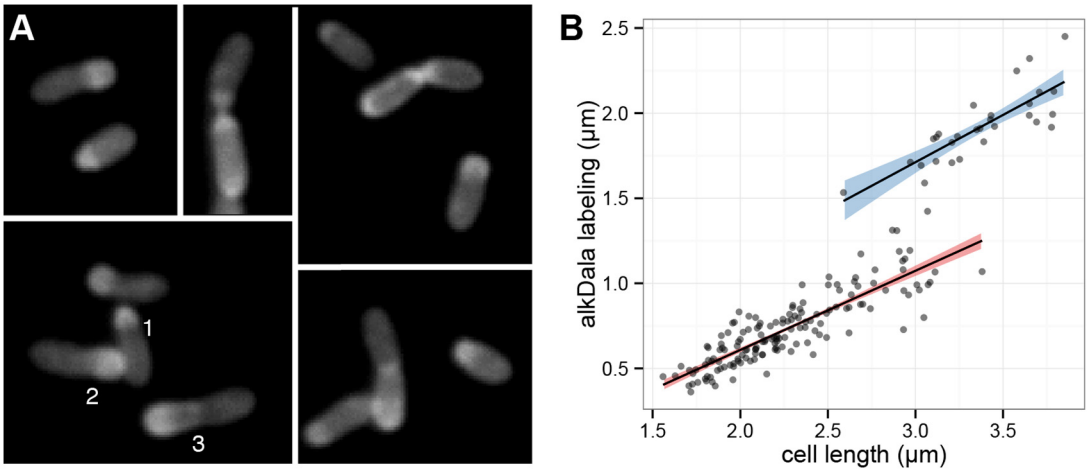

FIG 5 LDTs are active over an increasing area of the new cell compartment. (A) Individual cells were allowed to incorporate alkDala for 20 min. Shorter cells display a shorter region of labeling than longer cells; compare the labeling in cells 1 to 3. (B) Scatter plot of the length of the labeled region versus total cell length. The labeled region length increases linearly with cell length in cells before (red line) and after (blue line) the appearance of septal labeling in cells ~3.0 μm in length and longer. Red and blue shaded areas indicate 95% confidence intervals.

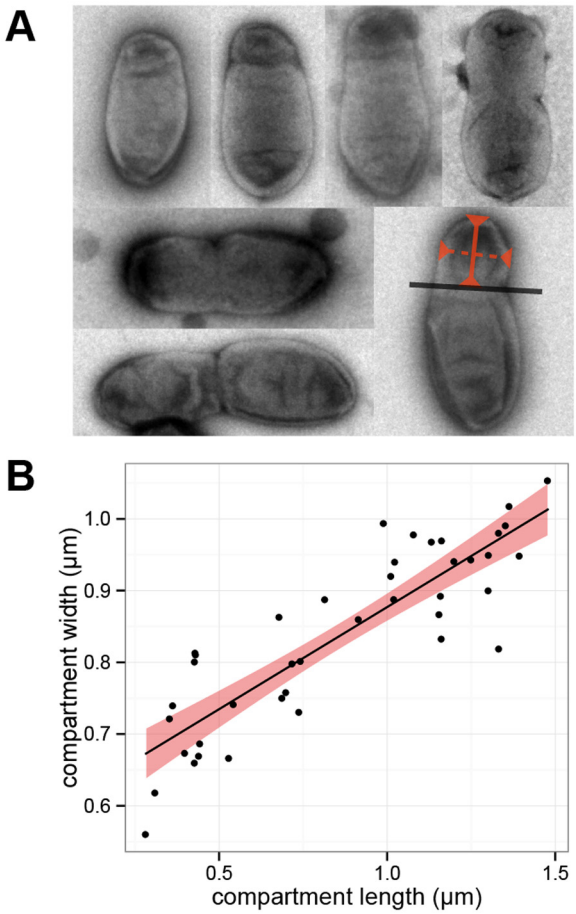

FIG 6 New cell compartments increase in width as they grow in length. (A) Examples of whole-cell TEM images of exponentially growing *A. tumefaciens*. Note the slight indentation/constriction (see also black line in lower right panel) demarking the boundary between the old and new cell compartments. (Lower right panel) Lengths and widths of new cell compartments (red) were measured. (B) Scatter plot of compartment lengths and widths of new cell compartments. The shaded area indicates the 95% confidence interval.

Polar growth involves expansion in cell width and length. The above results prompted us to examine the dimensions of *A. tumefaciens* over the cell cycle for evidence of growth that might correspond to the increased alkDala labeling area (Fig. 5B). New *A. tumefaciens* cell compartments frequently appeared to be narrower than their parent old cell compartments, even at the resolution afforded by light microscopy (see cells in Fig. 2A and C and 4A). Such new cell compartments presumably must eventually increase in width to maintain cell diameters over successive generations. However, it was not clear if this widening could be related to the observed increase in alkDala labeling.

To investigate changes in cell dimensions over the cell cycle, whole-cell transmission electron microscopy (TEM) was performed on mixed cultures of exponentially growing *A. tumefaciens*, and the lengths and widths of each new cell compartment were measured (Fig. 6A). Much like the alkDala labeling, there was a linear relationship between the lengths and widths of new cell compartments (Fig. 6B). Thus, although new poles are initially narrower than their parent old cell compartments, new cell compartments increase in both length and width as the cell matures. Furthermore, expansion of the new cell compartment corresponds to the increased area of alkDala labeling.

DISCUSSION

To better understand polar growth in the *Rhizobiales*, fluorescent fusions to predicted cell elongation and division components in *A. tumefaciens* were constructed. We refer to cell elongation and division proteins based on their canonical homologs in well-studied systems like *E. coli*. While the cell division scaffold proteins FtsZ and FtsA exhibited strong localization to the growth pole, the cell division-associated PBP3s did not. In contrast, the LDT Atu0845 displayed significant polar localization and may play a major role in polar growth. The latter finding is consistent with the unusual abundance of LDTs (see Fig. 3; see also Fig. S4 in the supplemental material) and LDT-mediated 3,3-cross-links in *A. tumefaciens* and other *Rhizobiales* (16). PBP1a, the only canonical cell elongation protein in *A. tumefaciens*, also exhibited only modest polar localization. Finally, polar growth was found to involve substantial cell shape remodeling and LDT-mediated PG synthesis activity over the entire new cell compartment.

A model of cell growth and division in *A. tumefaciens* is presented in Fig. 7. Cell elongation involves several stages during which a new cell compartment emerges and increases in length and width as it matures. Initially, the scaffold proteins FtsA and FtsZ localize to the growing pole tip along with PBP1a and LDT Atu0845. Over time, an increasing proportion of the new cell compartment engages in LDT-mediated PG synthesis activity (Fig. 7, red shading), implicating additional LDTs in this process. Prior to cell division, FtsZ leaves the growth pole before FtsA (Fig. 7), perhaps highlighting different functional roles for these proteins in polar growth. FtsZ, FtsA, PBP1a, PBP3s, and LDTs all localize to the midcell during cell division. Once the cell divides, the former septum becomes the site of new polar growth, utilizing the assortment of proteins already localized to the new pole.

In contrast to FtsZ of *E. coli*, FtsZ in *A. tumefaciens* appears to localize to the midcell prior to its membrane anchor FtsA (see Fig. 1). Similar results were reported for another alphaproteobacterium, *C. crescentus*, where FtsA arrives ~20 to ~25 min after FtsZ (35, 36). It is possible that *Alphaproteobacteria* possess a second unidentified FtsZ membrane anchor that acts in the early stages of septal FtsZ localization. This would not be surprising, given that both FtsA and the *Gammaproteobacteria*-specific ZipA function as membrane anchors in *E. coli* (37). Alternatively, the extended C-terminal domain of alphaproteobacterial FtsZ could help facilitate direct membrane interactions in the absence of an anchoring protein.

Polar growth in the *Rhizobiales* may have coevolved with the large number of LDTs within this order. The phylogenetic clustering of *Rhizobiales*- and *Rhodobacterales*-specific LDTs is particularly intriguing, since some members of *Rhodobacterales* also grow by budding. Unlike the *Rhizobiales*, the *Rhodobacterales* still retain MreB. However, MreB in *Rhodobacter sphaeroides* has atypical localization to the midcell (38), suggesting that *Rhodobacterales* may represent a growth strategy intermediate between the growth strategies of the polarly growing *Rhizobiales* and other *Alphaproteobacteria*. The phylogenetically divergent LDTs shared by these orders could help enable polar and other atypical growth in these organisms.

LDTs are also central components of the PG synthesis machinery in the Gram-positive, bipolarly growing *Actinomycetales*.

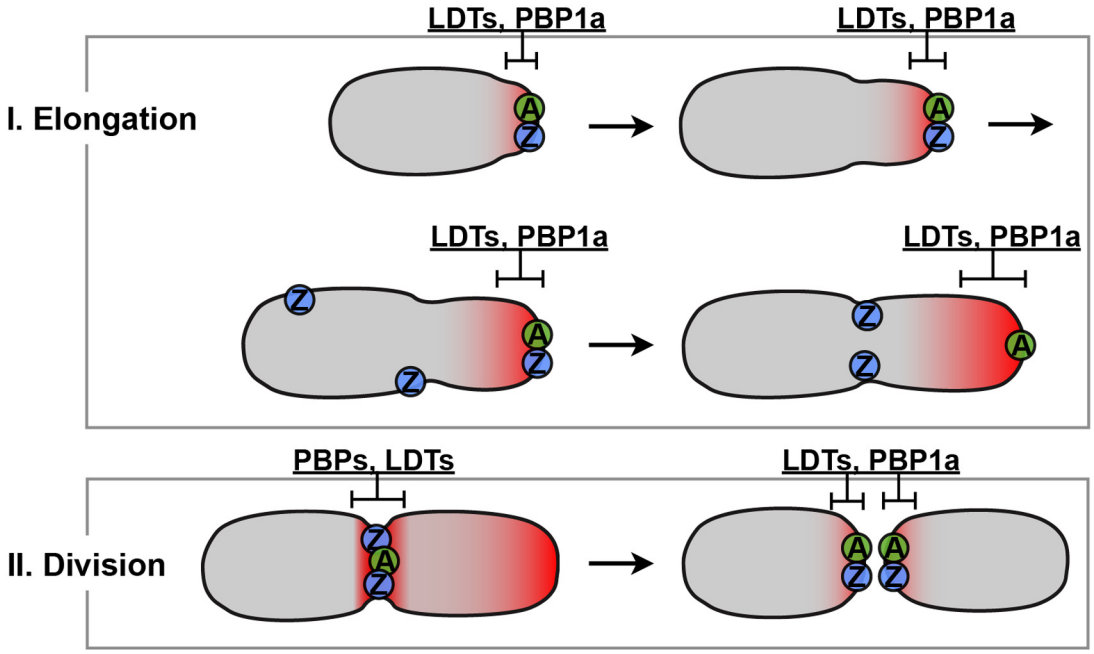

FIG 7 Model of *A. tumefaciens* cell growth dynamics and major protein localization over the cell cycle. The new cell compartment emerges from the new pole and gradually increases in length and width along with the region of active PG synthesis (red shading). FtsZ (blue "Z") and FtsA (green "A") localize to the growth pole along with PBP1a and the LDT Atu0845. Prior to cell division, FtsZ relocalizes to the septum, where it is joined by PBP3s, FtsA, PBP1a, and various LDTs for cell division. All these proteins remain at the division site and are ready to direct new cell polar growth in daughter cells. Square brackets illustrate the relative positions and lengths of regions of localization for LDTs and PBP1.

LDT-mediated 3,3-cross-links represent 38% of the PG cross-links in *Corynebacterium jeikeium* (39), 30% of those in *Mycobacterium smegmatis* (40), and 80% of those in *Mycobacterium tuberculosis* grown to stationary phase (41). In contrast, 3,3-cross-links represent less than 10% of the total cross-links in *E. coli* PG (27), and strains deleted of the LDTs exhibit no growth defects (42). The apparent association between polar growth and LDTs is intriguing and warrants future research to understand the nature of this relationship.

Polar growth is potentially influenced by one or more of the many well-studied mechanisms that control polar differentiation and the cell cycle in *Alphaproteobacteria*. For example, disruption or overexpression of CcrM, CpdR1, DivJ, DivK, PdhS1, PleC, or PodJ produces bulging, branching, and other cell shape and integrity defects in *Brucella abortus*, *S. meliloti*, or *A. tumefaciens* (43–48). Likewise, overexpression of the cell division protein MinCDE or FtsZ, or a partial deletion of MinCDE, generates swollen and branched cells in *S. meliloti* (49, 50). The similarity of the phenotypes during disruption of cell polarity, cell cycle, and cell growth proteins in numerous *Rhizobiales* may indicate a critical shared pathway that is sensitive to overexpression.

The mechanisms governing the insertion of nascent PG strands into established PG are not yet understood for any type of cell growth. Lateral expansion of the PG likely involves localized PG remodeling to allow insertion of new glycan strands into the existing PG mesh. However, because polar growth also involves a sustained expansion of the cell diameter, it may require considerably more PG synthesis and remodeling activity. Polar growth may represent a reversal of the highly regulated PG remodeling that occurs during cell division, where successively smaller rings of PG are generated at the septum (51–55). Since Atu0845 showed polar localization only during cell growth, additional LDTs are likely responsible for the PG synthesis and remodeling activities that lead to increased cell width. The results regarding subpolar PG synthesis imply that many aspects of polar growth in the *Rhizobiales* remain to be uncovered.

MATERIALS AND METHODS

Strains and growth conditions. Strains and plasmids used in this study are listed in Table S3 in the supplemental material. *A. tumefaciens* C58 containing nopaline pTiC58 was transformed with the plasmids described and cultured at 28°C on LB media supplemented with appropriate antibiotics. To obtain exponential growth, overnight cultures were diluted to ~10^8 cells/ml in LB containing 10 mM IPTG (isopropyl-β-D-thiogalactopyranoside) and antibiotics and then grown for 4 to 5 h at 28°C and 250 rpm prior to imaging. Note that fluorescent protein fusions were expressed at low levels from the pSRK-Km vector under these conditions (56); FtsZ-GFP expressed from this vector reaches only ~10% of native levels (20), and here we estimate that FtsA-GFP reaches only ~12.5% of native FtsA levels.

Cloning and genomic deletions. Plasmids were constructed using standard protocols, and all clones were verified by DNA sequencing. Strain ATC107 with Δ*pbp3b*::*npt* was constructed through allelic exchange by transforming wild-type C58 with pTC092, selecting for kanamycin-resistant clones, and then counterselecting for sucrose-resistant colonies using a protocol similar to that described by Kaniga et al. (57). Deletion of *pbp3b* was confirmed by PCR and sequencing.

Phylogenetic analyses. Phylogenetic trees of the PBP proteins were constructed by first gathering homologs to the *E. coli* K-12 PBP3 or PBP1b proteins within the desired species using Delta-BLAST (NCBI). Significant hits were roughly aligned using MAFFT (http://mafft.cbrc.jp/alignment/software/), and the PBP2/3 or PBP1a/b/c clusters were selected for a full alignment in MAFFT. LDT homologs were gathered on the basis of the ykud Pfam domain (http://pfam.sanger.ac.uk) and then aligned

using MAFFT. Columns containing more than 75% gaps were removed using trimAl (http://trimal.cgenomics.org). PhyML (http://www.atgc-montpellier.fr/phyml/) was used to calculate maximum-likelihood trees, using aLRT SH-like estimates of branch support. Trees were visualized using Archaeopteryx (version 0.9813; Christian Zmasek, Sanford-Burnham Medical Research Institute [http://www.phyloxml.org]) and Adobe Illustrator CS6 (Adobe Systems).

Fluorescence labeling. All centrifugations of cells were conducted for 5 min at 8,000 × *g*, and all manipulations were performed at room temperature unless otherwise noted. Cells were labeled with FM4-64 (Life Technologies) immediately prior to imaging by adding 8 mg/ml of FM4-64 to ~5×10^8 cells/ml in growth media and incubating for 10 min. Cells were centrifuged, and the supernatant was used to adjust to a final concentration prior to imaging. BocillinFL (Life Technologies) was added at a concentration of 167 μg/ml to cultures concentrated to ~10^9 cells/ml in LB. Cells were incubated at 28°C and 250 rpm for 10 min, pelleted, and washed twice with phosphate-buffered saline (PBS) (pH 7.4) and then labeled with FM4-64 as described.

Alkyne-D-alanine labeling was conducted essentially as previously described (34). In brief, (R)-a-propargylglycine (AlkDala; Fisher Scientific) was added to a final concentration of 1 mM to growing cultures of ~4×10^8 cells/ml and allowed to incorporate during 20 min of exponential growth. Cells were pelleted and washed once with pH 7.4 PBS–0.01% bovine serum albumin (BSA) (PBSB) and then fixed in ice-cold 70% ethanol for 20 min. After three additional washes, cells were incubated for 30 min in PBSB containing 1 mM copper sulfate, 128 μM Tris[(1-benzyl-1H-1,2,3-triazol-4-yl) methyl] amine (TBTA; Sigma-Aldrich), 1.3 mM copper sulfate, and 20 μM tetramethylrhodamine azide (TAMRA; Life Technologies). Cells were washed five times in PBSB prior to imaging.

For combined alkDala and Texas red succinimidyl ester (TRSE) labeling, cells were first concentrated to ~8×10^9 cells/ml in pH 8.5 PBS containing ~70 μg/ml TRSE (Life Technologies). After a 10-minute incubation, the reaction was quenched by addition of lysine to reach a concentration of 57 mM. Cells were washed once with LB and then resuspended to ~1.2×10^9 cells/ml with 1 mM alkDala. After 20 min of incubation at 28°C and 250 rpm, cells were washed three times with PBSB and fixed for 15 min in 2% formaldehyde. The remaining protocol was performed as described above except that Alexa Fluor 488 azide was used instead of TAMRA.

For combined vancomycin-FL and TRSE labeling, cells were resuspended to 4×10^8 cells/ml in LB and grown for 45 min following TRSE labeling. The culture was then concentrated to ~10^{10} cells/ml in LB, and vancomycin-BODIPY FL (Life Technologies) and unlabeled vancomycin were each added to reach a concentration of 10 ng/μl. Cells were incubated for 6 min and then washed twice prior to imaging.

Microscopy and data analysis. Slides were prepared by first covering a microscope slide with a thin (~340-μm-thick) layer of 1.5% agarose–PBS (pH 7.4). Once solidified, the agarose was trimmed to the size of a coverslip. Cells were resuspended at a final concentration of ~3×10^9 cells/ml, and then 2 μl was placed on top of each agarose pad, covered with a coverslip, and sealed with nail polish. Images were taken with an Applied Precision DeltaVision Elite deconvolution microscope and processed using Fiji/ImageJ (version 1.48; http://fiji.sc). Demographs were constructed by first measuring fluorescence intensity profiles in Fiji and then processing the data in R (version 3.0.2; R Foundation for Statistical Computing [http://www.r-project.org]) using a custom script designed to sort cells by length and normalize intensity profiles by each cell's average fluorescence. The script and a user guide are available at http://github.com/ta-cameron/Cell-Profiles. Demographs and all other plotted figures were generated in R using the ggplot2 package (version 0.9.3.1; Hadley Wickham, Department of Statistics, Rice University [http://ggplot2.org]).

Whole-cell TEM. Exponentially growing cultures were concentrated to ~8×10^9 cells/ml. Droplets of cell suspension were placed on Formvar-coated 200-mesh copper grids for 2 min. The grids were washed twenty times by passing them through drops of double-distilled water on parafilm. Excess water was wicked from the grids using filter paper. Grids were incubated with 5 μl of 0.5% uranyl acetate in water for 30 s; excess liquid was then wicked away using filter paper. Grids were air dried and subjected to electron microscopy using a Philips/Tecnai 12 TEM.

Homology searches. *E. coli* and *C. crescentus* cell growth and division protein sequences were used to search the *A. tumefaciens* genome with Delta-BLAST (NCBI) using a significance threshold of 0.05. Unambiguous hits with full-length alignments and good scores (greater than 80) were considered positive matches. In all other cases, Pfam was used to verify shared domain architectures between the query and top-scoring hits. In cases with multiple hits scoring similarly, all of the top hits sharing similar scores and domain architectures were included. Low-scoring and anomalous hits were considered low-confidence matches and marked as noted.

SUPPLEMENTAL MATERIAL

Supplemental material for this article may be found at http://mbio.asm.org/lookup/suppl/doi:10.1128/mBio.01219-14/-/DCSupplemental.

Figure S1, PDF file, 0.2 MB.
Figure S2, PDF file, 0.3 MB.
Figure S3, TIF file, 0.9 MB.
Figure S4, PDF file, 0.5 MB.
Figure S5, TIF file, 0.1 MB.
Figure S6, TIF file, 1.3 MB.
Figure S7, TIF file, 0.7 MB.
Table S1, PDF file, 0.1 MB.
Table S2, PDF file, 0.1 MB.
Table S3, PDF file, 0.1 MB.

ACKNOWLEDGMENTS

We thank Steve Ruzin and Denise Schichnes (Biological Imaging Facility, University of California, Berkeley) for assistance with microscopy and M. Sloan Siegrist and Carolyn R. Bertozzi (Department of Chemistry, University of California, Berkeley) for assistance with alkDala protocols and supplying Alexa Fluor 488 Azide.

J.A.-F. was partially supported by National Institutes of Health Genetics training grant GM007127. This research was supported by two National Science Foundation grants (to P.C.Z.), MCB-0923840 (American Recovery and Reinvestment Act Grant) and MCB-1243360.

REFERENCES

1. **Gan L, Chen S, Jensen GJ.** 2008. Molecular organization of gram-negative peptidoglycan. Proc. Natl. Acad. Sci. U. S. A. **105:**18953–18957. http://dx.doi.org/10.1073/pnas.0808035105.
2. **Beeby M, Gumbart JC, Roux B, Jensen GJ.** 2013. Architecture and assembly of the Gram-positive cell wall. Mol. Microbiol. **88:**664–672. http://dx.doi.org/10.1111/mmi.12203.
3. **Wang S, Furchtgott L, Huang KC, Shaevitz JW.** 2012. Helical insertion of peptidoglycan produces chiral ordering of the bacterial cell wall. Proc. Natl. Acad. Sci. U. S. A. **109:**E595–E604. http://dx.doi.org/10.1073/pnas.1117132109.
4. **Vollmer W, Seligman SJ.** 2010. Architecture of peptidoglycan: more data and more models. Trends Microbiol. **18:**59–66. http://dx.doi.org/10.1016/j.tim.2009.12.004.
5. **Cayley DS, Guttman HJ, Record MT.** 2000. Biophysical characterization of changes in amounts and activity of *Escherichia coli* cell and compartment water and turgor pressure in response to osmotic stress. Biophys. J. **78:**1748–1764. http://dx.doi.org/10.1016/S0006-3495(00)76726-9.
6. **Whatmore AM, Reed RH.** 1990. Determination of turgor pressure in *Bacillus subtilis*: a possible role for K+ in turgor regulation. J. Gen. Microbiol. **136:**2521–2526. http://dx.doi.org/10.1099/00221287-136-12-2521.
7. **den Blaauwen T, de Pedro MA, Nguyen-Distèche M, Ayala JA.** 2008. Morphogenesis of rod-shaped sacculi. FEMS Microbiol. Rev. **32:**321–344. http://dx.doi.org/10.1111/j.1574-6976.2007.00090.x.
8. **Vollmer W, Bertsche U.** 2008. Murein (peptidoglycan) structure, architecture and biosynthesis in *Escherichia coli*. Biochim. Biophys. Acta **1778:**1714–1734. http://dx.doi.org/10.1016/j.bbamem.2007.06.007.
9. **Li Y, Hsin J, Zhao L, Cheng Y, Shang W, Huang KC, Wang HW, Ye S.** 2013. FtsZ protofilaments use a hinge-opening mechanism for constric-

tive force generation. Science **341:**392–395. http://dx.doi.org/10.1126/science.1239248.
10. **Lan G, Daniels BR, Dobrowsky TM, Wirtz D, Sun SX.** 2009. Condensation of FtsZ filaments can drive bacterial cell division. Proc. Natl. Acad. Sci. U. S. A. **106:**121–126. http://dx.doi.org/10.1073/pnas.0911092106.
11. **Osawa M, Anderson DE, Erickson HP.** 2009. Curved FtsZ protofilaments generate bending forces on liposome membranes. EMBO J. **28:**3476–3484. http://dx.doi.org/10.1038/emboj.2009.277.
12. **Margolin W.** 2009. Sculpting the bacterial cell. Curr. Biol. **19:**R812–R822. http://dx.doi.org/10.1016/j.cub.2009.06.033.
13. **Swulius MT, Chen S, Jane Ding H, Li Z, Briegel A, Pilhofer M, Tocheva EI, Lybarger SR, Johnson TL, Sandkvist M, Jensen GJ.** 2011. Long helical filaments are not seen encircling cells in electron cryotomograms of rod-shaped bacteria. Biochem. Biophys. Res. Commun. **407:**650–655. http://dx.doi.org/10.1016/j.bbrc.2011.03.062.
14. **van Teeffelen S, Wang S, Furchtgott L, Huang KC, Wingreen NS, Shaevitz JW, Gitai Z.** 2011. The bacterial actin MreB rotates, and rotation depends on cell-wall assembly. Proc. Natl. Acad. Sci. USA **108:**15822–15827. http://dx.doi.org/10.1073/pnas.1108999108.
15. **Brown PJ, Kysela DT, Brun YV.** 2011. Polarity and the diversity of growth mechanisms in bacteria. Semin. Cell Dev. Biol. **22:**790–798. http://dx.doi.org/10.1016/j.semcdb.2011.06.006.
16. **Brown PJ, de Pedro MA, Kysela DT, Van der Henst C, Kim J, De Bolle X, Fuqua C, Brun YV.** 2012. Polar growth in the alphaproteobacterial order Rhizobiales. Proc. Natl. Acad. Sci. U. S. A. **109:**1697–1701. http://dx.doi.org/10.1073/pnas.1114476109.
17. **Kysela DT, Brown PJ, Huang KC, Brun YV.** 2013. Biological consequences and advantages of asymmetric bacterial growth. Annu. Rev. Microbiol. **67:**417–435. http://dx.doi.org/10.1146/annurev-micro-092412-155622.
18. **Jones LJ, Carballido-López R, Errington J.** 2001. Control of cell shape in bacteria: helical, actin-like filaments in *Bacillus subtilis*. Cell **104:**913–922. http://dx.doi.org/10.1016/S0092-8674(01)00287-2.
19. **Alyahya SA, Alexander R, Costa T, Henriques AO, Emonet T, Jacobs-Wagner C.** 2009. RodZ, a component of the bacterial core morphogenic apparatus. Proc. Natl. Acad. Sci. USA **106:**1239–1244. http://dx.doi.org/10.1073/pnas.0810794106.
20. **Zupan JR, Cameron TA, Anderson-Furgeson J, Zambryski PC.** 2013. Dynamic FtsA and FtsZ localization and outer membrane alterations during polar growth and cell division in *Agrobacterium tumefaciens*. Proc. Natl. Acad. Sci. U. S. A. **110:**9060–9065. http://dx.doi.org/10.1073/pnas.1307241110.
21. **van der Ploeg R, Verheul J, Vischer NO, Alexeeva S, Hoogendoorn E, Postma M, Banzhaf M, Vollmer W, Den Blaauwen T.** 2013. Colocalization and interaction between elongasome and divisome during a preparative cell division phase in *Escherichia coli*. Mol. Microbiol. **87:**1074–1087. http://dx.doi.org/10.1111/mmi.12150.
22. **Hocking J, Priyadarshini R, Takacs CN, Costa T, Dye NA, Shapiro L, Vollmer W, Jacobs-Wagner C.** 2012. Osmolality-dependent relocation of penicillin-binding protein PBP2 to the division site in *Caulobacter crescentus*. J. Bacteriol. **194:**3116–3127. http://dx.doi.org/10.1128/JB.00260-12.
23. **Varma A, Huang KC, Young KD.** 2008. The Min system as a general cell geometry detection mechanism: branch lengths in Y-shaped *Escherichia coli* cells affect Min oscillation patterns and division dynamics. J. Bacteriol. **190:**2106–2117. http://dx.doi.org/10.1128/JB.00720-07.
24. **Gullbrand B, Nordström K.** 2000. FtsZ ring formation without subsequent cell division after replication runout in *Escherichia coli*. Mol. Microbiol. **36:**1349–1359. http://dx.doi.org/10.1046/j.1365-2958.2000.01949.x.
25. **Young KD.** 2010. Bacterial shape: two-dimensional questions and possibilities. Annu. Rev. Microbiol. **64:**223–240. http://dx.doi.org/10.1146/annurev.micro.112408.134102.
26. **Magnet S, Dubost L, Marie A, Arthur M, Gutmann L.** 2008. Identification of the L,D-transpeptidases for peptidoglycan cross-linking in *Escherichia coli*. J. Bacteriol. **190:**4782–4785. http://dx.doi.org/10.1128/JB.00025-08.
27. **Glauner B, Höltje JV, Schwarz U.** 1988. The composition of the murein of *Escherichia coli*. J. Biol. Chem. **263:**10088–10095.
28. **Klüsener S, Hacker S, Tsai YL, Bandow JE, Gust R, Lai EM, Narberhaus F.** 2010. Proteomic and transcriptomic characterization of a virulence-deficient phosphatidylcholine-negative *Agrobacterium tumefaciens* mutant. Mol. Genet. Genomics **283:**575–589. http://dx.doi.org/10.1007/s00438-010-0542-7.
29. **Pédelacq JD, Cabantous S, Tran T, Terwilliger TC, Waldo GS.** 2006. Engineering and characterization of a superfolder green fluorescent protein. Nat. Biotechnol. **24:**79–88. http://dx.doi.org/10.1038/nbt1172.
30. **Dinh T, Bernhardt TG.** 2011. Using superfolder green fluorescent protein for periplasmic protein localization studies. J. Bacteriol. **193:**4984–4987. http://dx.doi.org/10.1128/JB.00315-11.
31. **Lam H, Oh DC, Cava F, Takacs CN, Clardy J, de Pedro MA, Waldor MK.** 2009. D-amino acids govern stationary phase cell wall remodeling in bacteria. Science **325:**1552–1555. http://dx.doi.org/10.1126/science.1178123.
32. **Cava F, de Pedro MA, Lam H, Davis BM, Waldor MK.** 2011. Distinct pathways for modification of the bacterial cell wall by non-canonical D-amino acids. EMBO J. **30:**3442–3453. http://dx.doi.org/10.1038/emboj.2011.246.
33. **Kuru E, Hughes HV, Brown PJ, Hall E, Tekkam S, Cava F, de Pedro MA, Brun YV, VanNieuwenhze MS.** 2012. In situ probing of newly synthesized peptidoglycan in live bacteria with fluorescent D-amino acids. Angew. Chem. Int. Ed. Engl. **51:**12519–12523. http://dx.doi.org/10.1002/anie.201206749.
34. **Siegrist MS, Whiteside S, Jewett JC, Aditham A, Cava F, Bertozzi CR.** 2013. (D)-Amino acid chemical reporters reveal peptidoglycan dynamics of an intracellular pathogen. ACS Chem. Biol. **8:**500–505. http://dx.doi.org/10.1021/cb3004995.
35. **Goley ED, Yeh YC, Hong SH, Fero MJ, Abeliuk E, McAdams HH, Shapiro L.** 2011. Assembly of the Caulobacter cell division machine. Mol. Microbiol. **80:**1680–1698. http://dx.doi.org/10.1111/j.1365-2958.2011.07677.x.
36. **Möll A, Thanbichler M.** 2009. FtsN-like proteins are conserved components of the cell division machinery in proteobacteria. Mol. Microbiol. **72:**1037–1053. http://dx.doi.org/10.1111/j.1365-2958.2009.06706.x.
37. **Pichoff S, Lutkenhaus J.** 2005. Tethering the Z ring to the membrane through a conserved membrane targeting sequence in FtsA. Mol. Microbiol. **55:**1722–1734. http://dx.doi.org/10.1111/j.1365-2958.2005.04522.x.
38. **Slovak PM, Wadhams GH, Armitage JP.** 2005. Localization of MreB in Rhodobacter sphaeroides under conditions causing changes in cell shape and membrane structure. J. Bacteriol. **187:**54–64. http://dx.doi.org/10.1128/JB.187.1.54-64.2005.
39. **Lavollay M, Arthur M, Fourgeaud M, Dubost L, Marie A, Riegel P, Gutmann L, Mainardi JL.** 2009. The beta-lactam-sensitive D,D-carboxypeptidase activity of Pbp4 controls the L,D and D,D transpeptidation pathways in Corynebacterium jeikeium. Mol. Microbiol. **74:**650–661. http://dx.doi.org/10.1111/j.1365-2958.2009.06887.x.
40. **Wietzerbin J, Das BC, Petit JF, Lederer E, Leyh-Bouille M, Ghuysen JM.** 1974. Occurrence of D-alanyl-(D)-meso-diaminopimelic acid and meso-diaminopimelyl-meso-diaminopimelic acid interpeptide linkages in the peptidoglycan of mycobacteria. Biochemistry **13:**3471–3476. http://dx.doi.org/10.1021/bi00714a008.
41. **Lavollay M, Arthur M, Fourgeaud M, Dubost L, Marie A, Veziris N, Blanot D, Gutmann L, Mainardi JL.** 2008. The peptidoglycan of stationary-phase *Mycobacterium* tuberculosis predominantly contains cross-links generated by L,D-transpeptidation. J. Bacteriol. **190:**4360–4366. http://dx.doi.org/10.1128/JB.00239-08.
42. **Sanders AN, Pavelka MS.** 2013. Phenotypic analysis of *Eschericia coli* mutants lacking L,D-transpeptidases. Microbiology **159:**1842–1852.
43. **Kahng LS, Shapiro L.** 2001. The CcrM DNA methyltransferase of *Agrobacterium tumefaciens* is essential, and its activity is cell cycle regulated. J. Bacteriol. **183:**3065–3075. http://dx.doi.org/10.1128/JB.183.10.3065-3075.2001.
44. **Kobayashi H, De Nisco NJ, Chien P, Simmons LA, Walker GC.** 2009. *Sinorhizobium meliloti* CpdR1 is critical for co-ordinating cell cycle progression and the symbiotic chronic infection. Mol. Microbiol. **73:**586–600. http://dx.doi.org/10.1111/j.1365-2958.2009.06794.x.
45. **Hallez R, Mignolet J, Van Mullem V, Wery M, Vandenhaute J, Letesson JJ, Jacobs-Wagner C, De Bolle X.** 2007. The asymmetric distribution of the essential histidine kinase PdhS indicates a differentiation event in *Brucella abortus*. EMBO J. **26:**1444–1455. http://dx.doi.org/10.1038/sj.emboj.7601577.
46. **Fields AT, Navarrete CS, Zare AZ, Huang Z, Mostafavi M, Lewis JC, Rezaeihaghighi Y, Brezler BJ, Ray S, Rizzacasa AL, Barnett MJ, Long SR, Chen EJ, Chen JC.** 2012. The conserved polarity factor podJ1 impacts multiple cell envelope-associated functions in *Sinorhizobium meliloti*. Mol. Microbiol. **84:**892–920. http://dx.doi.org/10.1111/j.1365-2958.2012.08064.x.
47. **Kim J, Heindl JE, Fuqua C.** 2013. Coordination of division and devel-

opment influences complex multicellular behavior in *Agrobacterium tumefaciens*. PLoS One **8:**e56682. http://dx.doi.org/10.1371/journal.pone.0056682.
48. **Pini F, Frage B, Ferri L, De Nisco NJ, Mohapatra SS, Taddei L, Fioravanti A, Dewitte F, Galardini M, Brilli M, Villeret V, Bazzicalupo M, Mengoni A, Walker GC, Becker A, Biondi EG.** 2013. The DivJ, CbrA and PleC system controls DivK phosphorylation and symbiosis in *Sinorhizobium meliloti*. Mol. Microbiol. **90:**54–71. http://dx.doi.org/10.1111/mmi.12347.
49. **Cheng J, Sibley CD, Zaheer R, Finan TM.** 2007. A *Sinorhizobium meliloti* minE mutant has an altered morphology and exhibits defects in legume symbiosis. Microbiology **153:**375–387. http://dx.doi.org/10.1099/mic.0.2006/001362-0.
50. **Latch JN, Margolin W.** 1997. Generation of buds, swellings, and branches instead of filaments after blocking the cell cycle of *Rhizobium meliloti*. J. Bacteriol. **179:**2373–2381.
51. **Heidrich C, Templin MF, Ursinus A, Merdanovic M, Berger J, Schwarz H, de Pedro MA, Höltje JV.** 2001. Involvement of *N*-acetylmuramyl-L-alanine amidases in cell separation and antibiotic-induced autolysis of *Escherichia coli*. Mol. Microbiol. **41:**167–178. http://dx.doi.org/10.1046/j.1365-2958.2001.02499.x.
52. **Priyadarshini R, Popham DL, Young KD.** 2006. Daughter cell separation by penicillin-binding proteins and peptidoglycan amidases in *Escherichia coli*. J. Bacteriol. **188:**5345–5355. http://dx.doi.org/10.1128/JB.00476-06.
53. **Priyadarshini R, de Pedro MA, Young KD.** 2007. Role of peptidoglycan amidases in the development and morphology of the division septum in *Escherichia coli*. J. Bacteriol. **189:**5334–5347. http://dx.doi.org/10.1128/JB.00415-07.
54. **Peters NT, Dinh T, Bernhardt TG.** 2011. A fail-safe mechanism in the septal ring assembly pathway generated by the sequential recruitment of cell separation amidases and their activators. J. Bacteriol. **193:**4973–4983. http://dx.doi.org/10.1128/JB.00316-11.
55. **Yang DC, Tan K, Joachimiak A, Bernhardt TG.** 2012. A conformational switch controls cell wall-remodelling enzymes required for bacterial cell division. Mol. Microbiol. **85:**768–781. http://dx.doi.org/10.1111/j.1365-2958.2012.08138.x.
56. **Khan SR, Gaines J, Roop RM, Farrand SK.** 2008. Broad-host-range expression vectors with tightly regulated promoters and their use to examine the influence of TraR and TraM expression on Ti plasmid quorum sensing. Appl. Environ. Microbiol. **74:**5053–5062. http://dx.doi.org/10.1128/AEM.01098-08.
57. **Kaniga K, Delor I, Cornelis GR.** 1991. A wide-host-range suicide vector for improving reverse genetics in gram-negative bacteria: inactivation of the blaA gene of Yersinia enterocolitica. Gene **109:**137–141. http://dx.doi.org/10.1016/0378-1119(91)90599-7.